NACA RM L57A03

NACA

RESEARCH MEMORANDUM

INVESTIGATION OF THE EFFECT OF VELOCITY DIAGRAM ON INLET TOTAL-PRESSURE DISTORTIONS THROUGH SINGLE-STAGE SUBSONIC AXIAL-FLOW COMPRESSORS

By George C. Ashby, Jr.

Langley Aeronautical Laboratory
Langley Field, Va.

NATIONAL ADVISORY COMMITTEE
FOR AERONAUTICS

WASHINGTON

April 17, 1957
Declassified October 14, 1957

NACA RM L57A03

NATIONAL ADVISORY COMMITTEE FOR AERONAUTICS

RESEARCH MEMORANDUM

INVESTIGATION OF THE EFFECT OF VELOCITY DIAGRAM ON INLET TOTAL-PRESSURE DISTORTIONS THROUGH SINGLE-STAGE SUBSONIC AXIAL-FLOW COMPRESSORS

By George C. Ashby, Jr.

SUMMARY

A preliminary theoretical and experimental investigation of the effect of velocity diagram on inlet total-pressure distortions through single-stage subsonic axial-flow compressors for incompressible flow has been conducted. As a result of the theoretical investigation, velocity diagrams with an included angle of 90° between the absolute and relative flow directions either at the inlet or exit (with flow coefficient not greater than 0.5) were indicated to be optimum for elimination of total-pressure distortion by a compressor stage. When an included angle is 90°, loading (turning angle) has no apparent influence; however, for included angles less than 90°, the loading should be low.

For the experimental tests, the wake of a 1/4-inch-diameter rod was measured upstream of the rotor. By using the measured upstream wake and a derived equation for incompressible flow, the wake downstream of the rotor was estimated and compared with the measured downstream wake for several velocity diagrams.

The rod wakes of the experimental tests were of such small circumferential extent that the undistorted flow dictated the static-pressure field in the blade passage. Equilibrium with this pressure field required a smaller radius of curvature for the distorted flow and resulted in greater turning and therefore greater energization than that estimated. However, for inlet total-pressure distortions which extend far enough circumferentially to alter the static-pressure field in the blade passage, the derived equation will estimate the downstream distortion with reasonable accuracy.

INTRODUCTION

One of the most important problems associated with high-speed gas-turbine aircraft is reduced compressor and therefore engine performance resulting from inlet total-pressure distortions. The flow distortions may occur when the engine is operated at off-design condition, when the aircraft is flown at high angles of attack, or when the flow is turned or diffused too rapidly within the diffuser. At supersonic speeds when the engine is operated at off-design condition or when the aircraft is flown at high angles of attack, a distorted flow may result because of nonuniform compression at the inlet throat. At subsonic speeds with either the off-design or high-angle-of-attack condition, a distorted flow may result because of flow separation from the inlet lip. When the flow is turned or diffused too rapidly within the diffuser ducting, a flow distortion results because of separation from the walls (ref. 1).

One approach to the solution of the inlet total-pressure-distortion problem is to reduce the distortion before it reaches the compressor. References 1 and 2 show that total-pressure distortions at the compressor inlet may be reduced when better mixing is provided in the inlet ducting by increasing the diffuser length, by contracting the exit of the diffuser, or by using screens or freely rotating fans. Internal boundary-layer bleed at the inlet throat will also reduce the distortion.

Another approach is to design the compressor to withstand better the effects of the distortion. A preliminary investigation of the velocity diagrams of representative inlet stages shows that in general total-pressure distortion will be reduced across a rotor because the distorted flow or low-energy region is energized more than the undistorted flow by the rotor.

The purpose of the present investigation is to determine which type of velocity diagram is most effective in reducing total-pressure distortions. The results were experimentally verified by the introduction of a small disturbance upstream of a compressor stage.

SYMBOLS

c_p	specific heat of air at constant pressure, ft-lb/slug-$^\circ$R
c_v	specific heat of air at constant volume, ft-lb/slug-$^\circ$R
H	total enthalpy, $\left(u + \frac{P}{\rho}\right)$ ft-lb/slug

u	internal energy, ft-lb/slug
p	static pressure, lb/sq ft
P	total pressure, lb/sq ft
dP	total-pressure difference between undistorted flow and point in distorted flow, lb/sq ft
q	dynamic pressure, $\frac{1}{2}\rho V^2$, lb/sq ft
R	gas constant, ft-lb/slug-$^{\circ}$R
U	blade speed, ft/sec
V	velocity, ft/sec
ΔV_t	change in tangential velocity across rotor, ft/sec
φ	flow coefficient, $\frac{V_a}{U}$
α	angle of attack relative to blade chord, $\beta_{1R} - \xi$, deg
β	flow angle measured from axis of rotation, deg
θ	turning angle, $\beta_{1R} - \beta_{2R}$, deg
ξ	blade-setting angle (angle between blade chord and axis of rotation), deg
ρ	air density, slugs/cu ft

Subscripts:

i	upstream of guide vane
1	upstream of rotor
2	downstream of rotor
a	axial direction
d	design condition
R	relative coordinates
t	tangential direction

ANALYSIS

The velocity diagrams analyzed are shown in figure 1. In these diagrams, the distorted flow velocities (dashed line) are superimposed on the undistorted flow velocities (solid line). The analysis was made on the basis of incompressible flow with the following assumptions:

1. The undistorted and distorted flows enter the rotor with the same absolute direction.

2. The static pressure of the distorted and undistorted flows is equal at the inlet and also at the exit of the rotor.

3. The increase of blade angle of attack in the distorted flow is not sufficient to cause blade stall.

4. The distorted flow is turned in the rotor passage to the same exit direction, relative to the rotor, as the undistorted flow $\left(\frac{d\theta}{d\alpha} = 1.0\right)$.

Figure 1(a) is the velocity diagram of a rotor alone with an undistorted-flow inlet-air angle of 45° (β_{1R}). Both the distorted and undistorted flows enter the rotor axially. Since the blade speed is constant, the extremities of the inlet relative-velocity vectors of the two flows lie along a line parallel to the inlet absolute vectors. The inlet relative-velocity vector of the distorted flow, compared with that of the undistorted flow, has a smaller magnitude, produces a larger inlet-air angle (β_{1R}), and therefore a greater angle of attack $(\beta_{1R} - \xi)$ to the rotor blade. Under assumption 4, the two flows exit relative to the rotor in the same direction. Assumption 2 regarding static pressure, and the difference in magnitude between the inlet relative velocities require that the magnitude of the exit relative velocity be less for the distorted flow. Because the static pressures are equal, the difference in total pressure between the two flow regions is proportional to the difference between the squares of their absolute velocities. For this diagram (fig. 1(a)), the distortion has been reduced approximately 50 percent by the rotor.

Figure 1(b) is the velocity diagram of a guide-vane—rotor combination. The guide vane turns the flow 30° in the direction of rotor rotation and the rotor has an undistorted-flow inlet-air angle of 60°. Since the included angle between the inlet flow directions on the absolute and relative frames of reference is 90° $(\beta_{1R} + \beta_1 = 90^\circ)$, the inlet relative-velocity vector of the undistorted flow is perpendicular to the line along which lie the extremities of the inlet relative-flow vectors (V_{1R}) of both flows. Therefore, the inlet relative-flow vectors of both flows will be approximately the same length for distortions which do not produce a large

change in the relative inlet-air angle. A change of 8° in inlet-air angle due to a distortion will result in a difference in relative velocity of 1 percent. The static pressure of these two streams is equal; therefore, the total pressures relative to the rotor are equal. Both flows are turned to the same relative exit direction and, because of the required equality of static pressure, the vectors are coincident. The vectors are also coincident in the absolute frame of reference, and, therefore, the exit total pressures are the same. For this diagram, under the assumptions made, the distortion would be eliminated by the first stage. It is noted that a significant parameter for the elimination of the distortion in the first stage of a compressor is the included angle between the relative and absolute flow directions entering the rotor.

An included angle of 90° between the relative and absolute flow directions is also significant when it occurs at the exit of the rotor (as evidenced by fig. 1(c)). This velocity diagram is for a rotor alone with an undistorted-flow inlet-air angle (β_{1R}) of 64°. The analysis of inlet flow for this diagram is the same as that for the diagram of figure 1(a). The turning angle has been selected so that the angle between the relative and absolute flow direction leaving the rotor is 90° $\left(\beta_{2R} + \beta_2 = 90^\circ\right)$. Thus, with the same reasoning being used as in figure 1(b), the absolute velocities in the distorted and in the undistorted flow regions are approximately equal. Because of uniform static pressure for the two flows, the total pressures of the flows are equal. The difference in the absolute flow angle can be rectified by the stator and the distortion will be eliminated by the first stage.

From the velocity diagram, it can also be seen that the deficit in total pressure between the distorted and undistorted flow is reduced because the distorted flow is energized by the rotor more than is the undistorted flow. This is manifested by the larger change in tangential velocity across the rotor for the distorted flow. By using the well-known equation for the energy added by the rotor

$$H_2 - H_1 = U_2 V_{t,2} - U_1 V_{t,1} \tag{1}$$

and the assumptions used for the velocity-diagram analysis, the difference between the total pressures of the undistorted flow and distorted flow after passing through the rotor can be expressed in terms of the flow angles. The resulting equation, the derivation of which is given in the appendix, for incompressible flow is

$$dP_2 = dP_1 \left[\cos\left(\beta_1 + \beta_{1R}\right) \cos\left(\beta_2 + \beta_{2R}\right) \frac{\cos \beta_1}{\cos \beta_{1R}} \frac{\cos \beta_{2R}}{\cos \beta_2} \right] \tag{2}$$

When the total-pressure deficit between the undistorted flow and a point in the distorted flow upstream of the rotor and the velocity diagram for the undistorted flow is known, the downstream total-pressure deficit can be determined by using this equation.

Dr. Leroy H. Smith, Jr., of the General Electric Company, in a discussion with the author at the Langley Laboratory, proffered an equation for the variation in energy added by the rotor with respect to $V_1^2/2$. His equation, derived under the same assumptions, can be reduced to equation (2). (This information has recently been published (see ref. 3).)

Equation (2) verifies the analysis of the velocity diagrams. It can be seen that if either or both of the included angles $(\beta_1 + \beta_{1R})$ and $(\beta_2 + \beta_{2R})$ is 90°, the total-pressure deficit between the distorted and undistorted flows will be eliminated. If one of the included angles is greater than 90°, the total-pressure deficit will be negative. The rotor, therefore, more than made up the total pressure needed to raise the distorted-flow total pressure to that of the undistorted flow. It is interesting to note that if both of the included angles are greater than 90°, the deficit will not be completely eliminated. When the velocity diagram has neither of the included angles equal to 90°, the decrease in the inlet total-pressure distortion across the rotor depends not only on the size of the inlet and exit included angles but also on the relative size of the absolute and relative flow angles at the inlet and at the exit; that is, the larger the ratios of $\frac{\beta_1}{\beta_{1R}}$ and $\frac{\beta_{2R}}{\beta_2}$, the greater will be the decrease in the distortion for given included angles. The inlet total-pressure distortion could increase across the rotor if the included angles were very small, and if β_1 and β_{2R} were much smaller than β_{1R} and β_2, respectively. The analysis has been given in terms of the flow angles of the velocity diagram. However, the velocity diagram is the end result of a compressor-stage design, and an analysis in terms of the design parameters, flow coefficient (φ), and loading (turning angle) would be of more interest to the designer. Considering the conclusions of the analysis with respect to these parameters, it is found that for an included angle $(\beta_R + \beta)$ of 90° the flow coefficient (φ) reaches a maximum of 0.5 when $\beta_R = \beta = 45°$. The flow coefficient would have to be less than 0.5 for an included angle to be greater than 90°. When an included angle is 90°, there is no apparent influence of loading on the amount of distortion elimination since the $\frac{\cos \beta_{2R}}{\cos \beta_2}$ term of equation (2), which increases as loading (turning angle) increases, has no influence. However, for included angles other than 90°, both the flow coefficient and loading influence the amount of distortion elimination.

The entering flow coefficient (φ_1) in conjunction with the guide-vane exit angle (β_1) establishes the entering included angle. The exiting flow coefficient (φ_2) in conjunction with the loading (turning angle) determines the downstream included angle. Since included angles approaching 90° are desired, the flow coefficient should be kept in the vicinity of 0.5. For given values of flow coefficients, since β_1 and loading (turning angle) establish the values of the $\frac{\cos \beta_1}{\cos \beta_{1R}}$ and $\frac{\cos \beta_{2R}}{\cos \beta_2}$ terms, respectively, of equation (2), the guide-vane turning should be high and the loading low.

EXPERIMENTAL TESTS

In order to check the results of the analysis of the velocity diagrams, the wake of a 1/4-inch-diameter rod was measured upstream and downstream of a rotor.

Apparatus

A schematic diagram of the 28-inch test compressor is presented in figure 2. The flow enters from the atmosphere through a honeycomb straightener and three screens. An entrance cone with a contraction ratio of 13:1 is used to accelerate the flow into the test section. The rotor discharges through an annular diffuser. Downstream of the annular diffuser the flow is turned outward through a radial diffuser which can be adjusted to decrease or increase the exit area and thus regulate the flow rate. The drive is a 75-horsepower direct-current motor operable from 0 to 2,400 rpm. The design details of the rotor are given in reference 4. The rotor blades had medium-camber NACA 65-$(C_{l_o}A_{10})10$ airfoil sections. The blade chord at the mean radius was 3.0 inches, and the solidity was 1.0 from root to tip. The rotor-tip radius was 13.91 inches and the hub-tip radius ratio was 0.784. The rotor blades were attached to the hub with threaded blade shanks, and lock nuts to allow changes in the blade-setting angle to be made. The guide vane had a constant NACA 65-series airfoil section with zero twist from hub to tip. The chord and solidity at the mean radius were 2.5 inches and 1.0, respectively. Each blade was attached to the outer casing with a single screw allowing variations in blade-setting angle to be made.

Instrumentation

The measuring stations are shown in figure 2. Several rod ports were spaced circumferentially at station i. A prism probe, described in reference 5, was used to determine the dynamic pressure at station i. A 26-tube total-pressure rake, figure 3(a), was used to measure the rod wake and a prism probe was used to measure dynamic pressure and flow direction upstream of the rotor at station 1. A 25-tube shielded total-pressure rake, figure 3(b), was used to measure the rod wake, and a prism probe was used to measure the dynamic pressure and flow direction downstream of the rotor at station 2. The tubes of the downstream rake were shielded and inclined 40° counterclockwise from the axial direction in order to make the rake insensitive to changes in the exit-flow angle and to provide measurements an equal distance behind the rotor trailing edge. All measurements were made at the mean radius.

Test Program and Procedure

Three rotor-alone and two rotor—guide-vane configurations at a solidity of 1.0 were used to produce various velocity diagrams. For the rotor-alone configurations, the blade-setting angles, measured at the mean radius, were $\xi_d = 40^\circ$ and $\xi_d \pm 7.5^\circ$. For the rotor—guide-vane configurations, the blade-setting angle was 7.5° above design, and the guide vane was set to turn the flow 30° in the direction of rotor rotation and also 25° in the opposite direction. Several throttle settings were used for each configuration to provide comparisons at various angles of attack. The rotor speed for all tests was 2,000 rpm. For each test, the rod wake was first measured upstream. The upstream rake and prism probe were located close to the outer casing to prevent interference while the downstream measurements were made. In order to insure that the downstream rake measured the total rod wake, measurements were made with the rod in several circumferential locations approximately 1 inch apart.

Presentation of Data

All of the wakes are plotted as the ratio of the difference between the total pressure of the undistorted flow and a point in the distorted flow to the dynamic pressure at station i as a function of circumferential distance measured from the center of the wake. Because of mixing losses, the integrated total-pressure deficit between the wake and the undistorted flow would increase as the wake moved downstream. Measurements of the rod wake in a straight duct show that, between measuring positions corresponding to those in the test $\left(5\frac{1}{4}\right.$ inches and $\left.11\frac{1}{4}\right.$ inches downstream of the rod$\Big)$, the integrated total-pressure deficit would increase by 4.0 percent.

Since this change is so small and since the rotor is expected to decrease the integrated total-pressure deficit by 30 to 100 percent, comparisons across the rotor based on $\frac{dP}{q_i}$ will suffice for this report. The integrated deficit will differ at the leading edge and at the trailing edge of the blade from those at the upstream and downstream measuring stations, respectively; however, the differences would be less than 4.0 percent and can be considered insignificant.

RESULTS AND DISCUSSION

Figure 4 presents the rod wake measured upstream and downstream of the rotor, together with the downstream wake estimated using equation (2), for the five configurations at approximately design angle of attack. The downstream wakes were measured on the rake with the rod in several circumferential positions. A different symbol is used for each rod position. The test points both upstream and downstream are located with respect to the center of the wake. The plots are arranged from the top of the figure in the order of increasing wake elimination, based on the ratio of the area under the estimated downstream curve to the area under the measured upstream curve. The percentages of wake elimination in the order of presentation are 39.3, 39.5, 57.7, 80.5, and 100 (figs. 4(a) to 4(e)), respectively. For all configurations, the measured wakes decrease across the rotor and the percentages of wake elimination, in the order presented in figure 4, are 64.4, 57.0, 77.0, 96.7, and 64.9, respectively. The rotor eliminated a greater portion of the wake than estimated, with one exception; for the rotor-alone configurations, the trend of increasing wake elimination follows that estimated. The reason for the difference between the estimated and measured percentage of elimination will be explained subsequently. For the rotor—guide-vane configurations (figs. 4(b) and 4(e)), considerable variation between the wakes measured for the several circumferential positions of the rod is evident. Some of the variation may be due to the change of circumferential position of the rod wake relative to the guide-vane blades. It should be noted that the estimated downstream wakes were calculated for these tests assuming that the streamlines enter and leave the rotor at the same radius, whereas the tests are three dimensional. (Equation (2) applies to three-dimensional flow if the streamline path is known.) The rotor-alone configurations would be closer to two-dimensional flow than the rotor—guide-vane configurations, because the rotor was designed for two-dimensional flow without a guide vane, and the guide vane was not designed for use with this rotor. The mismatching of the rotor and guide vane leads to more pronounced radial flow shifts which alter the shape of the wake across the rotor considerably as manifested in the downstream curves. For the rotor-alone configurations (figs. 4(a), 4(c), and 4(d)), the effects are small, as evidenced at the extremities of the downstream

wakes, and the wakes measured at the several circumferential positions coincide. The rotor-alone configuration at angles of attack considerably above design, for which flow shifts are more pronounced, show differences between wake measurements at the various circumferential positions and shape alteration of the wakes across the rotor similar to those of figure 4(e). An example of this is shown in figure 5(c). Figure 5 presents plots for the rotor alone at design blade-setting angle and angles of attack of $\alpha_d - 6.8^\circ$, α_d, and $\alpha_d + 7.5^\circ$. The measured wake is reduced across the rotor for all angles of attack and follows the same trend as that estimated with respect to increasing percentage of wake elimination with increasing angle of attack.

Considering the rotor-alone plots (since they are closer to two-dimensional flow) in figures 4 and 5, it is noted that, since the measured wake elimination follows the estimated trend, the experimental results verify the conclusion of the theoretical analysis; that is, the degree of distortion elimination is a function of the size of the angles of the velocity diagram. Contrary to prediction of the velocity-diagram analysis, the velocity diagram with one included angle approximately 90° and the other slightly larger than 90° failed to eliminate the distortion completely because of three-dimensional effects; however, the three rotor-alone tests of figure 4 provide some proof that a 90° included angle may be optimum for eliminating a distortion across a stage. For these three velocity diagrams, the value of the bracketed term of equation (2), excluding the exit included-angle term, $\cos(\beta_2 + \beta_{2R})$, had values of 1.01, 0.98, and 0.94 for figures 4(a), 4(c), and 4(d), respectively. These values represent the ratio of the integrated estimated downstream wake to the integrated upstream wake. The percentages of wake elimination for the three diagrams are therefore -1.0 percent, 2.0 percent, and 6.0 percent. The differences between the three configurations are small whereas the estimated values, including the exit included-angle term, are 39.3 percent, 57.7 percent, and 80.5 percent. The larger differences between the three configurations indicate that the predominant term is the exit included angle. The measured percentages of wake elimination for the three diagrams, 64.4, 77.0, and 96.7 for exit included angles of 51.1°, 64.3°, and 79.0°, respectively, have differences between them of the same order as those between the estimated values; therefore, the advantage of the exit included angle approaching 90° is evident.

As noted previously, the measured wake was reduced a greater amount than that estimated; therefore, the wake was energized to a greater extent than calculated. A reappraisal of the initial assumptions upon which equation (2) was based shows that, in order to produce a greater work input than estimated, either a greater diffusion occurs in the wake $\left(p_{2\text{distortion}} > p_2\right)$ or the low-energy air experiences a greater turning than that assumed $\left(\frac{d\theta}{d\alpha} > 1.0\right)$. The existence of a difference between the

static pressure in a wake and in the surrounding flow is contrary to experience; therefore, the low-energy air must have been overturned. Since the rotor is subjected to the angles of attack in the wake for a short period of time, the static-pressure field in the blade passage is dictated by the undistorted flow. Therefore, because the relative velocity of the wake particles is lower than that of the undistorted flow, the wake particles will not be in equilibrium with the surrounding pressure field unless the radius of curvature is smaller at all points. The net result is an overturning of the distorted flow.

There are indications that this overturning is true. As blade-setting angle or undistorted-flow angle of attack increases, the difference between the relative velocities of the two flows becomes smaller and less difference in radius of curvature is required to maintain equilibrium. As blade-setting angle (fig. 4) and angle of attack (fig. 5) increases, the measured wake is more nearly equal to that estimated. At this point, it should be noted that equation (2) would estimate the downstream wake more accurately for inlet flow distortions which are of large enough circumferential extent to alter the static-pressure field in the blade passage if the angle of attack in the distorted flow is not large enough to cause blade stall.

CONCLUSIONS

A preliminary theoretical and experimental investigation of the effect of velocity diagram on inlet total-pressure distortions through single-stage subsonic axial-flow compressors for incompressible flow has been conducted. The wake of a 1/4-inch-diameter rod, measured both upstream and downstream of a rotor, has been compared for various velocity diagrams. The measured downstream wake was also compared with the downstream wake estimated by using a derived equation subject to the assumptions that (a) the undistorted and distorted flows enter the rotor with the same absolute direction, (b) the static pressures of the undistorted and distorted flows are equal at the inlet and also at the exit of the rotor, (c) the increase of blade angle of attack in the distorted flow is not sufficient to cause blade stall, and (d) the distorted flow is turned in the rotor passage to the same exit direction, relative to the rotor, as the undistorted flow. As a result of this investigation, the following conclusions are made:

1. Velocity diagrams for which the included angle between the relative and absolute flow directions is 90°, at either the inlet or exit of the rotor, are indicated to be optimum for eliminating inlet total-pressure distortions across the first stage of a compressor. A flow coefficient of 0.5 or less is required, but loading (turning angle) has no apparent influence.

2. Velocity diagrams, with one of the included angles greater than 90°, will increase the total pressure of the distortion beyond that of the undistorted total pressure. However, if both included angles are greater than 90°, the inlet total-pressure distortion will not be completely eliminated. For these results, either or both the entering and exiting flow coefficients must be less than 0.5.

3. When the velocity diagram has neither of the included angles equal to 90°, the decrease in the inlet total-pressure distortion across the rotor depends not only on the size of the inlet and exit included angles but also on the relative size of the absolute and relative flow angles at the inlet and at the exit. Both flow coefficient and loading influence the amount of distortion elimination. The flow coefficient should not be too much greater than 0.5, the guide-vane exiting angle should be high, and the loading should be low for the greatest elimination of distortion by the rotor.

4. The experimental tests show that the derived equation will estimate the downstream distortion with reasonable accuracy for inlet total-pressure distortion which extends far enough circumferentially to alter the static-pressure field in the blade passage.

Langley Aeronautical Laboratory,
National Advisory Committee for Aeronautics,
Langley Field, Va., December 11, 1956.

APPENDIX

DETERMINATION OF THE EQUATION FOR ESTIMATING THE TOTAL-PRESSURE DIFFERENCE BETWEEN THE UNDISTORTED FLOW AND A POINT IN THE DISTORTED FLOW AFTER THE FLOW HAS PASSED THROUGH THE ROTOR

The equation for the energy added by the rotor is

$$H_2 - H_1 = U_2 V_{t,2} - U_1 V_{t,1} \tag{A1}$$

where $H = u + \frac{P}{\rho}$.

For incompressible flow

$$H_2 - H_1 = \frac{c_v}{R\rho}\left(p_2 - p_1\right) + \frac{P_2 - P_1}{\rho} \tag{A2}$$

Equating (A1) and (A2) and rearranging gives

$$\frac{P_2}{\rho} = \frac{P_1}{\rho} + U_2 V_{t,2} - U_1 V_{t,1} - \frac{c_v}{R\rho}\left(p_2 - p_1\right) \tag{A3}$$

The total-pressure difference between the undistorted flow and a point in the distorted flow entering the rotor is a function of the difference in the squares of the absolute velocities; therefore, the variation in total pressure between the two flow regions downstream of the rotor will be determined with respect to $V_1^2/2$.

In order to write the variables of equation (A3) in terms of $V_1^2/2$, it can be seen from figure 1(b) that

$$V_{t,1} = \sqrt{2}\sqrt{V_1^2/2}\sin\beta_1 \tag{A4}$$

$$V_{t,2} = U_2 - V_{2R}\sin\beta_{2R} \tag{A5a}$$

The velocity V_{2R} in terms of $V_1^2/2$ can be obtained from the relative enthalpy rise, which is

$$H_{2R} - H_{1R} = \frac{U_2^2 - U_1^2}{2} = \frac{c_p}{R\rho}\left(p_2 - p_1\right) + \frac{V_{2R}^2}{2} - \frac{V_{1R}^2}{2} \qquad \text{(A5b)}$$

Then, by rearranging equation (A5b) and substituting

$$V_{1R}^2 = U_1^2 - 2U_1\sqrt{2}\sqrt{V_1^2/2}\sin\beta_1 + 2\left(V_1^2/2\right)$$

The velocity V_{2R} in terms of $V_1^2/2$ is as follows:

$$V_{2R} = \sqrt{U_2^2 - 2U_1\sqrt{2}\sqrt{V_1^2/2}\sin\beta_1 + 2\left(V_1^2/2\right) - \frac{2c_p}{R\rho}\left(p_2 - p_1\right)} \qquad \text{(A5c)}$$

Substituting equation (A5c) into equation (A5a) results in

$$V_{t,2} = U_2 - \sin\beta_{2R}\sqrt{U_2^2 - 2U_1\sqrt{2}\sqrt{V_1^2/2}\sin\beta_1 + 2\left(V_1^2/2\right) - \frac{2c_p}{R\rho}\left(p_2 - p_1\right)} \qquad \text{(A5d)}$$

Combining equations (A3), (A4), and (A5d) gives

$$\frac{P_2}{\rho} = \frac{P_1}{\rho} + U_2^2 - U_2\sin\beta_{2R}\sqrt{U_2^2 - 2U_1\sqrt{2}\sqrt{V_1^2/2}\sin\beta_1 + 2\left(V_1^2/2\right) - \frac{2c_p}{R\rho}\left(p_2 - p_1\right)} - U_1\sqrt{2}\sqrt{V_1^2/2}\sin\beta_1 - \frac{c_v}{R\rho}\left(p_2 - p_1\right) \qquad \text{(A6)}$$

Taking the derivative of equation (A6) with respect to $V_1^2/2$ results in

$$\frac{dP_2}{d\left(V_1^2/2\right)} = \frac{dP_1}{d\left(V_1^2/2\right)} + \rho\left[\frac{\left(U_2\sin\beta_{2R}\right)\left(U_1\sin\beta_1\right)}{V_{2R}V_1} - \frac{U_2\sin\beta_{2R}}{V_{2R}} - \frac{U_1\sin\beta_1}{V_1}\right] \qquad \text{(A7)}$$

Multiplying both sides of equation (A7) by $d\left(V_1^2/2\right)$ and substituting $\rho\, d\left(V_1^2/2\right) = dq_1 = dP_1$ gives

$$dP_2 = dP_1\left[1 + \frac{\left(U_2 \sin \beta_{2R}\right)\left(U_1 \sin \beta_1\right)}{V_{2R}V_1} - \frac{U_2 \sin \beta_{2R}}{V_{2R}} - \frac{U_1 \sin \beta_1}{V_1}\right] \quad (A8)$$

Multiplying the appropriate terms by $\frac{V_{a1}}{V_{a1}}$ or $\frac{V_{a2}}{V_{a2}}$ and substituting $\cos \beta = \frac{V_a}{V}$ and $\cos \beta_R = \frac{V_a}{V_R}$ results in the following equation:

$$dP_2 = dP_1\left[1 + \left(\frac{U_2}{V_{a2}} \cos \beta_{2R} \sin \beta_{2R}\right)\left(\frac{U_1}{V_{a1}} \cos \beta_1 \sin \beta_1\right) - \frac{U_2}{V_{a2}} \cos \beta_{2R} \sin \beta_{2R} - \frac{U_1}{V_{a1}} \cos \beta_1 \sin \beta_1\right] \quad (A9)$$

Substituting $\frac{U}{V_a} = \frac{\sin \beta}{\cos \beta} + \frac{\sin \beta_R}{\cos \beta_R}$ in equation (A9), using the identity $\cos\left(\beta + \beta_R\right) = \cos \beta \cos \beta_R - \sin \beta \sin \beta_R$, and rearranging gives

$$dP_2 = dP_1\left[\cos\left(\beta_1 + \beta_{1R}\right) \cos\left(\beta_2 + \beta_{2R}\right) \frac{\cos \beta_1}{\cos \beta_{1R}} \frac{\cos \beta_{2R}}{\cos \beta_2}\right] \quad (A10)$$

This is the equation for the total-pressure deficit between the undistorted flow and a point in the distorted flow after the flow has passed through the rotor. If the upstream total-pressure deficit and the velocity diagram for the undistorted flow is known, the downstream total-pressure deficit can be obtained.

REFERENCES

1. Piercy, Thomas G., and Klann, John L.: Experimental Investigation of Methods of Improving Diffuser-Exit Total-Pressure Profiles for a Side-Inlet Model at Mach Number 3.05. NACA RM E55F24, 1955.

2. Sterbentz, William H.: Factors Controlling Air-Inlet Flow Distortions. NACA RM E56A30, 1956.

3. Smith, L. H., Jr.: Recovery Ratio - A Measure of the Loss Recovery Potential of Compressor Stages. Paper No. 56 - A-206, A.S.M.E. (Presented at ASME Annual Meeting, New York, Nov. 25-30, 1956.)

4. Ashby, George C., Jr.: Comparison of Low-Speed Rotor and Cascade Performance for Medium-Camber NACA 65-$\left(C_{l_o} A_{10}\right)10$ Compressor-Blade Sections Over a Wide Range of Rotor Blade-Setting Angles at Solidities of 1.0 and 0.5. NACA RM L54I13, 1954.

5. Schulze, Wallace M., Ashby, George C., Jr., and Erwin, John R.: Several Combination Probes for Surveying Static and Total Pressure and Flow Direction. NACA TN 2830, 1952.

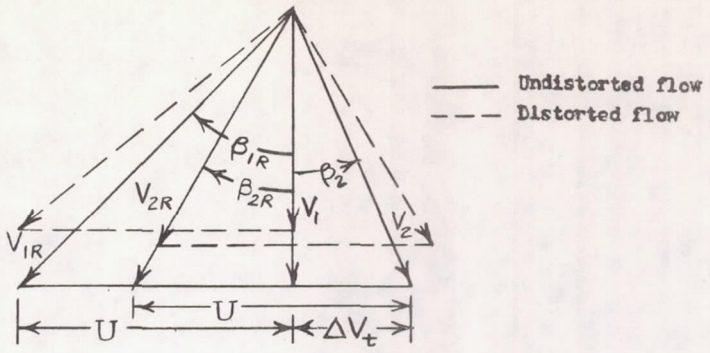

(a) Rotor alone; $\beta_{1R} = 45^\circ$ in undistorted flow.

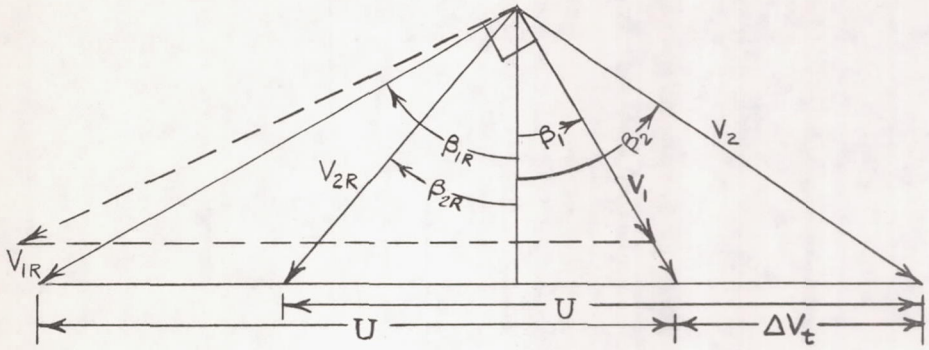

(b) Rotor with guide vane; $\beta_1 = 30^\circ$; $\beta_{1R} = 60^\circ$ in undistorted flow $\left((\beta_{1R} + \beta_1) = 90^\circ\right)$.

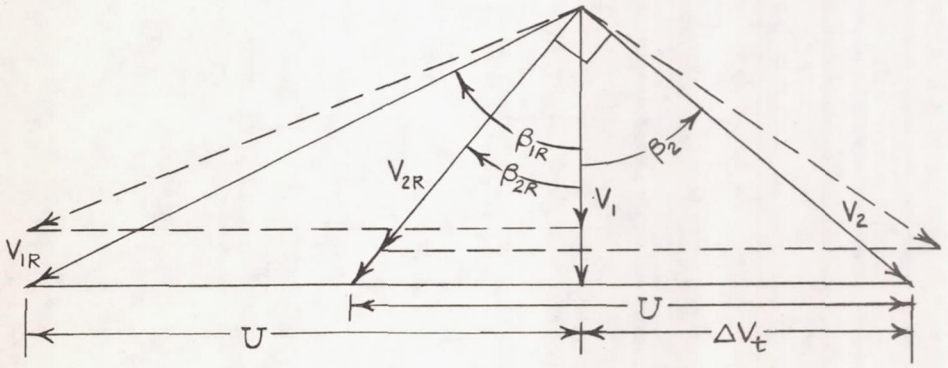

(c) Rotor alone; $\beta_{1R} = 64^\circ$ in undistorted flow $\left((\beta_{2R} + \beta_2) = 90^\circ\right)$.

Figure 1.- Velocity diagrams.

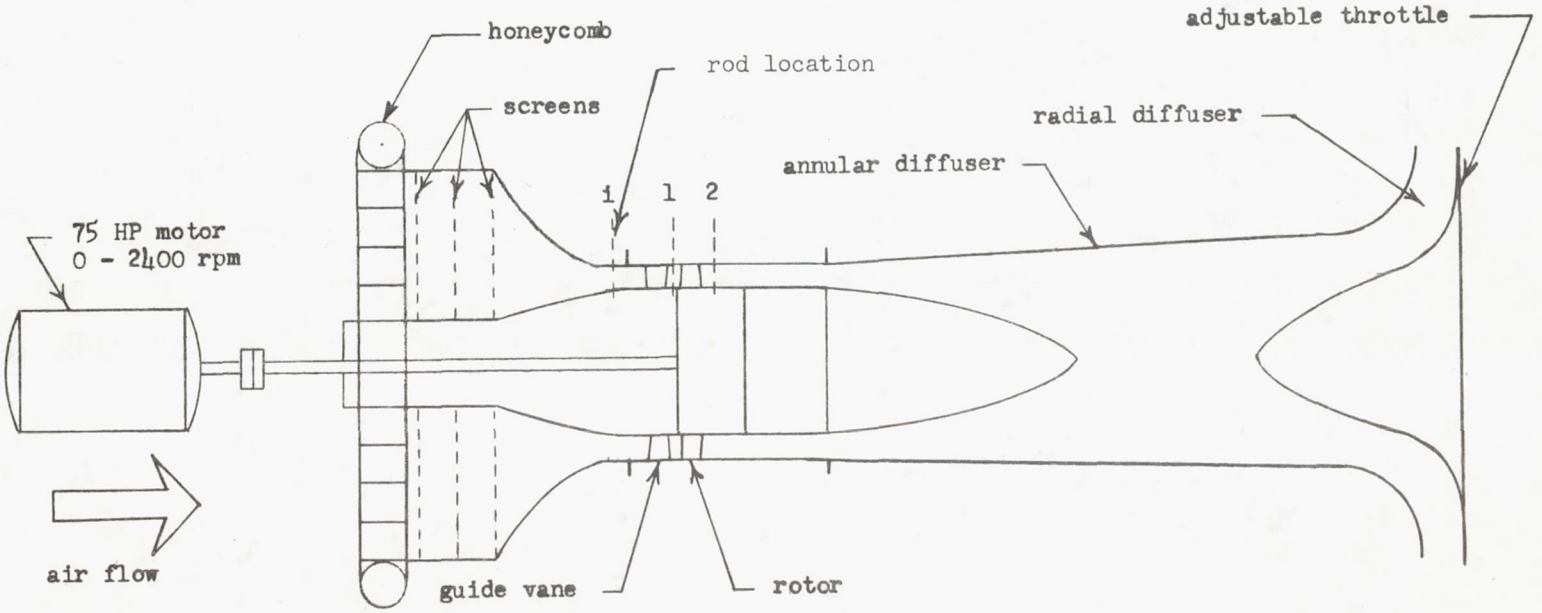

Figure 2.- Schematic diagram of test compressor showing blade rows and instrumentation positions.

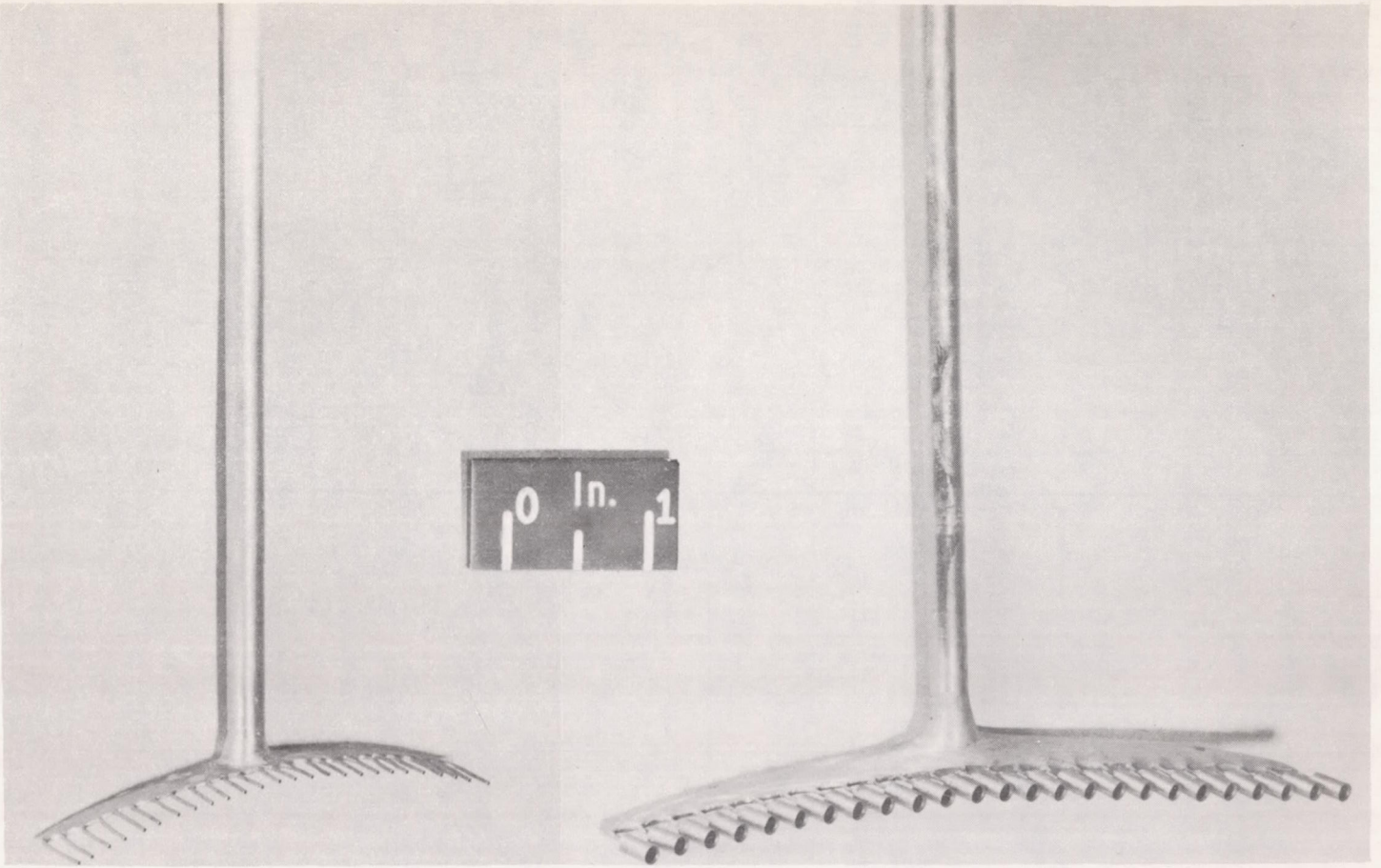

(a) Upstream rake. (b) Downstream rake. L-95911

Figure 3.- Rakes used to measure rod wake upstream and downstream of rotor.

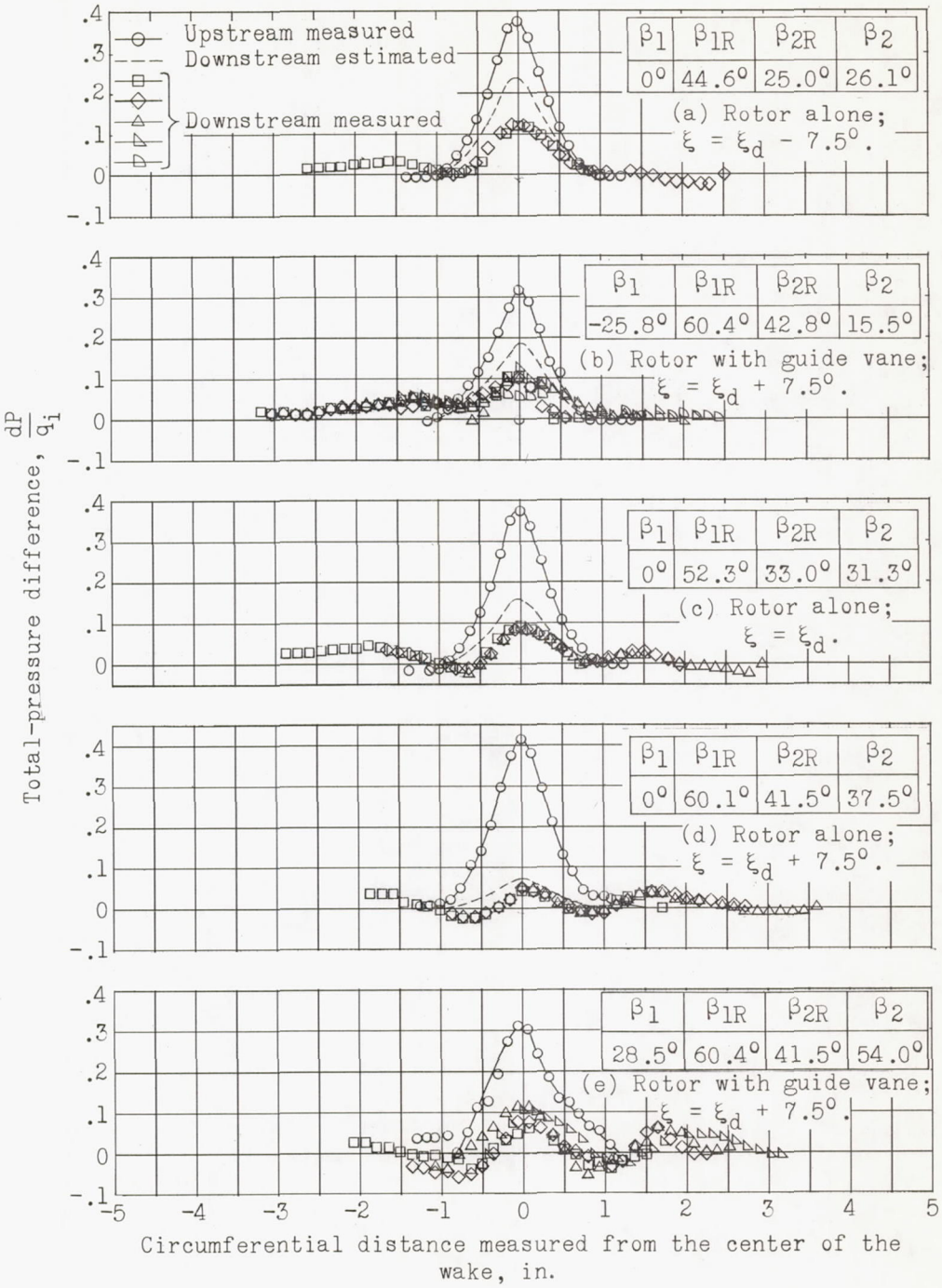

Figure 4.- Comparison of measured and estimated downstream rod wakes with the measured upstream wake for five test configurations at approximately design angle of attack.

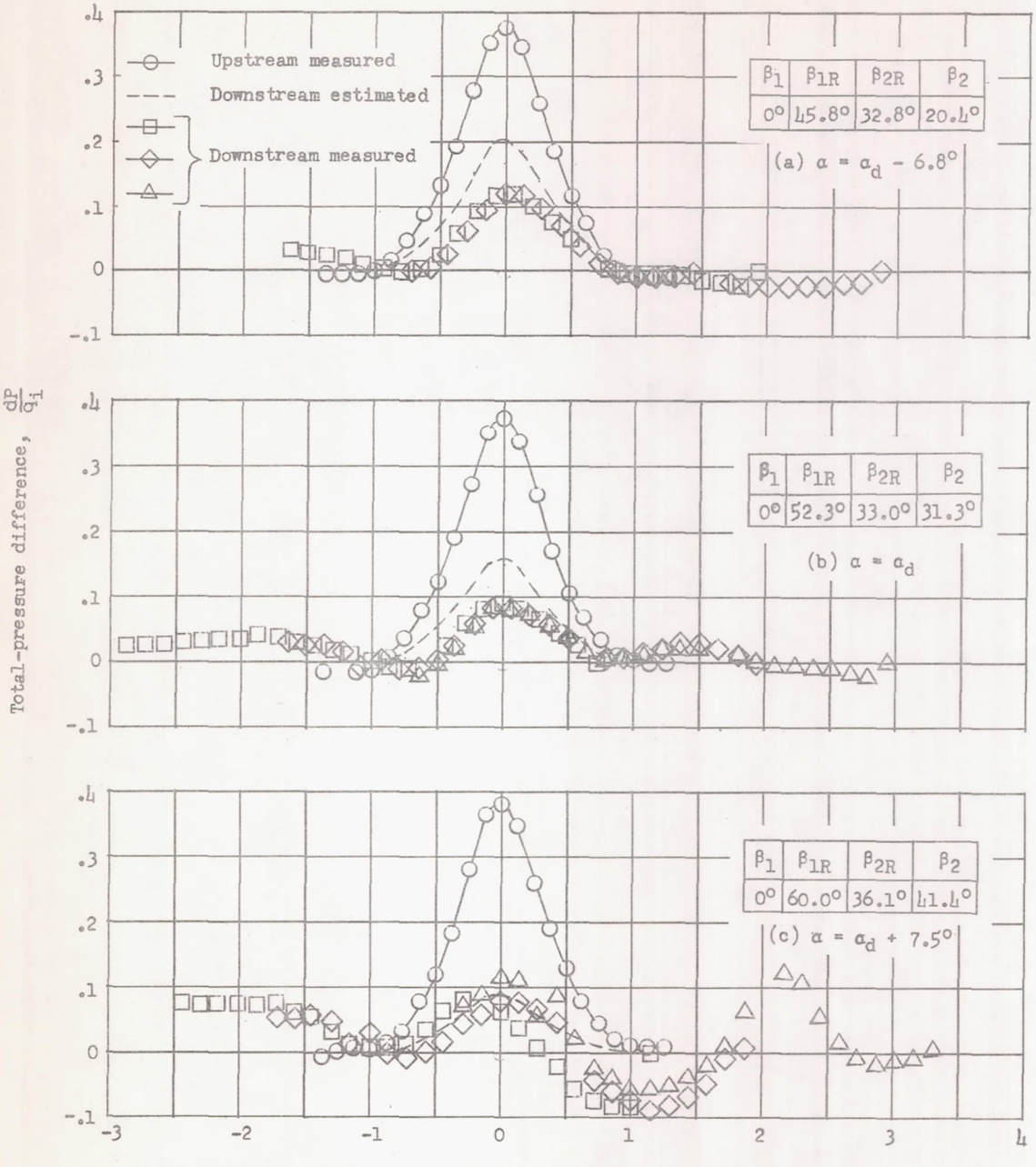

Figure 5.- Comparison of measured and estimated downstream rod wakes with measured upstream wake for rotor alone; $\xi = \xi_d$; configuration at three angles of attack.